Tuning the response of fluid filled hydrogel core-shell

structures

Michal Levin<sup>a</sup>, Megan T. Valentine<sup>b</sup>, and Noy Cohen<sup>a</sup>, and

<sup>a</sup>Department of Materials Science and Engineering, Technion – Israel Institute of Technology, Haifa 3200003, Israel

<sup>b</sup>Department of Mechanical Engineering, University of California, Santa Barbara, CA 93106, USA

Abstract

Hydrogels are hydrophilic polymer networks that swell upon submersion in water. Thanks to their bio-compatibility, compliance, and ability to undergo large deformations, hydrogels can be used in a wide variety of applications such as in situ sensors for measuring cell-generated forces and drug delivery vehicles. In this work we investigate the equilibrium mechanical responses that can be achieved with hydrogel-based shells filled with a liquid core. Two types of gel shell geometries are considered - a cylinder and a spherical shell. Each shell is filled with either water or oil and subjected to compressive loading. We illustrate the influence of the shell geometry and the core composition on the mechanical response of the structure. We find that all core-shell structures stiffen under increasing compressive loading due to the load-induced expulsion of water molecules from the hydrogel shell. Furthermore, we show that cylindrical core-shell configurations are stiffer then their spherical equivalents. Interestingly, we demonstrate that the compression of a core-shell structure with an aqueous core leads to the transportation of water molecules from the core into the hydrogel. These results will guide the

\*e-mail address: valentine@engineering.ucsb.edu

†e-mail address: noyco@technion.ac.il

design of novel core-shell structures with tunable properties and mechanical responses.

## 1 Introduction

Hydrogels are formed by the submersion of a loosely cross-linked and highly hydrophilic polymer network in water. Water influx causes the 3-dimensional network to expand substantially by swelling, as compared to its dehydrated volume, rather than dissolve (Ullah et al., 2015; Varaprasad et al., 2017). The swelling process is driven by a difference in the chemical potential of solvent molecules inside and outside the gel (Flory, 1953). In addition, swelling is characterized by the stretching of polymer chains in order to make room for the water molecules (Cohen and McMeeking, 2019). The equilibrium swollen configuration of the gel is achieved when mechanical and chemical equilibriums are reached. The latter is achieved when the difference in the chemical potential of water molecules inside and outside the gel vanishes.

Hydrogels are an important class of bio-compatible soft materials that are well established for use in wound healing (Boateng et al., 2008; Kamoun et al., 2017; Gupta et al., 2019) and tissue replacement (Lee and Mooney, 2001; Drury and Mooney, 2003; Hoffman, 2012; Jagur-Grodzinski, 2006; Li and Mooney, 2016), owing to their tunable mechanical properties, low cell cytotoxicity, selective permeability, and the ability to functionalize the hydrogel surface to control gel:cell interactions. Hydrogels are critically important for the encapsulation and controlled release of a wide range of therapeutic compounds (Graham and McNeill, 1984; Gupta et al., 2002; Duncan, 2003; Dreiss, 2020). They are also increasingly used in regenerative medicine and cell therapies to provide appropriate physiochemical environments for delivery or implantation of islet, stem, or progenitor cells into tissues of interest (Xu et al., 2019; Wang et al., 2018; Choe et al., 2018; Burdick et al., 2016). Hydrogel mechanics in particular are known to be critically important in proliferation and differentiation of encapsulated stem cells (Banerjee et al., 2009; Lee et al., 2013; Engler et al., 2006).

This class of materials also hold promise as in situ sensors of cell-generated boundary forces (see Ribeiro et al. (2016); Huang et al. (2016); Roca-Cusachs et al. (2017); Vorselen et al. (2020))

that are known to regulate critical cell functions ranging from receptor signaling and transcription to differentiation and proliferation (Mendez and Janmey, 2012; Uroz et al., 2018; Franck et al., 2011). The large majority of traction force measurements have been performed using compliant planar hydrogels to which isolated cells attach (Huang et al., 2012; Munevar et al., 2001). While these have provided critical information regarding the structures and mechanisms of cell force sensing, the 2D geometry causes cells to maximize adherence area and adopt highly polarized shapes, thus limiting their relevance to physiological conditions. To meet this need, we and others (Vorselen et al., 2020; Mohagheghian et al., 2018; Kaytanlı et al., 2020) are developing new strategies to measure the full 3D deformations of compressible polymeric hydrogel microspheres to which cells can apply both shear and normal forces, which we call microsphere-based traction force microscopy ( $\mu$ TFM). Unlike methods that study isolated cells within bulk hydrogel matrices,  $\mu$ TFM maintains native cell-cell contacts and allows multi-cellular aggregates and tissues to be studied with minimal perturbation. Moreover, hydrogel microspheres can sustain shear, allowing cells to naturally interact with neighboring cells, while their finite compressibility allows measurement of both the anisotropic deviations in the boundary tractions and the isotropic (hydrostatic) pressure (Kaytanlı et al., 2020).

Critical to the deployment of these hydrogel-based devices and sensors in biological and medical settings is the ability to control the hydrogel mechanics. In general, hydrogel stiffness influences adhesion, motility, and other functions of cells that contact the gel. In the case of  $\mu$ TFM, it sets the range of detectable traction forces due to the limited optical resolution of fluorescence microscopy, which is used to measure the boundary deformation. One challenge in the general use of hydrogels is the limited range of mechanical responses that can be developed using homogeneous, single-phase gels. Recent advances in droplet-based microfluidics provide an avenue to manufacturing multiphase core-shell particles with a hydrogel-based shell and a liquid core which contains one or more internal inclusions (Xu and Nisisako, 2020; Nisisako and Hatsuzawa, 2016; Ran et al., 2017). In principle, such a method can expand the design palette for hydrogel materials for use in delivery,

encapsulation, and sensing. Through careful design of the hydrogel based core-shell composition and properties, we demonstrate that we can tune the mechanical response of hydrogels to enhance their performance in a variety of applications. For example, such methods can be used to match the properties of hydrogel based cell sensors to the tissues in which they are deployed, or to provide a perturbative input to test the tissue response. Moreover, the liquid core provides an opportunity to store payload molecules, including therapeutics, which can then be delivered upon tissue-generated compression (Ran et al., 2017; Mahdavi et al., 2020).

In this work we investigate the response of hydrogel-based core-shell composites to external loading, following the works of Drozdov (2015) and Cohen (2019). We begin by summarizing the theoretical background. We then consider the mechanical response of spherical or cylindrical hydrogel shells that are filled with a liquid core of either water, which can permeate the shell, or oil, which cannot. Using simulations of structures with different dimensions, geometries, and compositions, we demonstrate the wide range of mechanical responses that can be achieved through hydrogel composite design and provide a design framework for the development of hydrogel materials optimized for specific applications.

# 2 Theoretical background

During the manufacturing of fluid-filled polymeric gels using microfluidics methods, the gel and its fluid core are generally co-formed (Xu and Nisisako, 2020; Ran et al., 2017; Mahdavi et al., 2020). However, to model the properties that can be achieved using this process we artificially divide the fabrication process into two phases. First, we consider a dry polymeric shell that swells in the presence of water molecules. Subsequently, we "fill" the shell with a liquid, leading to a fluid filled polymeric hydrogel. We follow by applying an external load which forces the expulsion of water molecules from the hydrogel, resulting in its dehydration and stiffening. This mechanism is observed in biological systems such as the liquefaction of the vitreous body of the eye (Levin and Cohen, 2021).

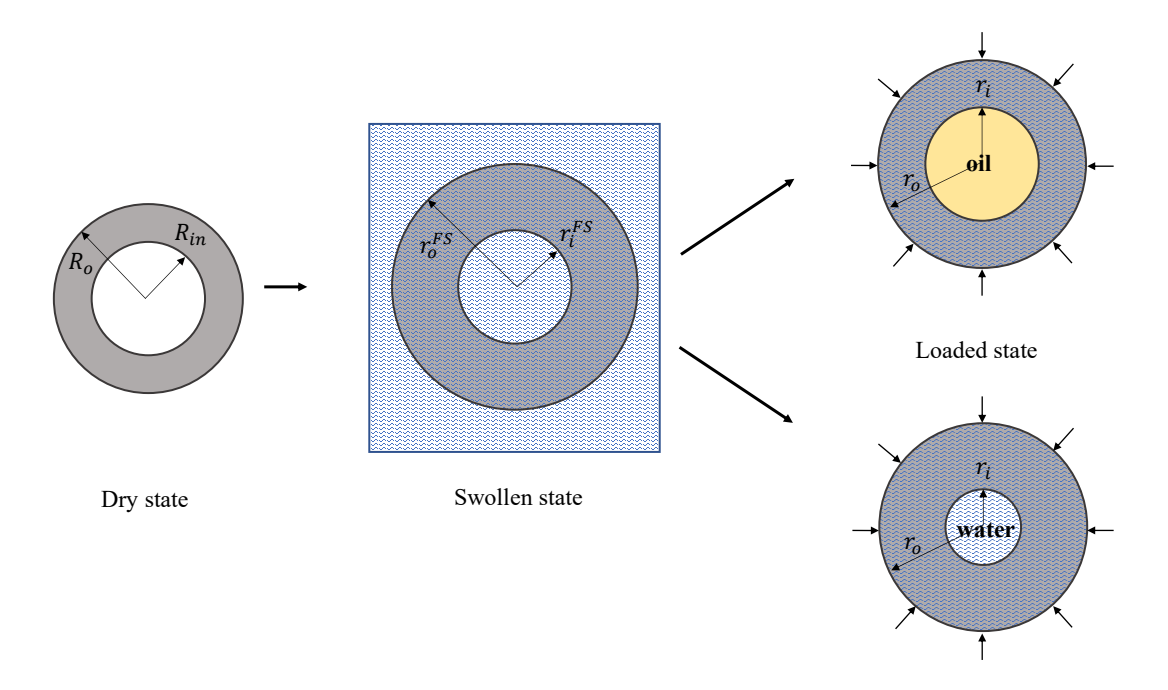


Figure 1: Illustration of the dry, the swollen, and the loaded configurations.

Accordingly, we begin by considering a dry incompressible hydrophilic polymeric shell comprising  $N_0$  randomly oriented and uniformly distributed chains per unit referential volume, where each chain is made of n repeat units (or monomers). The total volume of the polymer is approximated via  $V_p = n N_0 v_p$ , where  $v_p$  is the volume of a monomer. The location of the referential material points in the dry configuration are denoted by  $\mathbf{x}$ .

The polymer shell is submerged in a water bath at temperature T and pressure  $\tilde{p}$  and allowed to swell. We refer to the configuration in which chemical and mechanical equilibrium is reached as the swollen state. Here,  $\tilde{m}$  liquid molecules diffuse into the gel such that its total volume is  $\tilde{V}_g = V_p + \tilde{m} \, v_l$ , where  $v_l$  is the volume of a water molecule. The material points are denoted by  $\tilde{\mathbf{x}}$  and we define the deformation gradient from the reference to the swollen state by  $\tilde{\mathbf{F}} = \partial \tilde{\mathbf{x}}/\partial \mathbf{x}$ . Assuming that the liquid and the polymer segments are incompressible, the total volumetric change due to the free swelling process is  $\tilde{J} = \det \tilde{\mathbf{F}} = \tilde{V}_g/V_p$ . We follow by filling the swollen polymeric shell with either water or oil and sealing it.

Next, the swollen polymeric shell is subjected to a quasi-static external loading that results in

the migration of liquid molecules into or out of the gel to achieve an equilibrium configuration. We denote the volume of the gel in the loaded state by  $V_g = V_p + m v_l$ , where m is the number of liquid molecules in equilibrium. The material points are denoted by  $\mathbf{y}$  and accordingly we define the deformation gradient from the swollen to the loaded state by  $\mathbf{F}_l = \partial \mathbf{y}/\partial \tilde{\mathbf{x}}$ . The ratio between the volumes in the swollen and the loaded state is  $J_l = \det \mathbf{F}_l$ .

For completeness, we denote that the deformation gradient from the reference to the loaded state is  $\mathbf{F} = \mathbf{F}_l \tilde{\mathbf{F}}$ . The total volumetric deformation  $J = \det \mathbf{F} = V_g/V_p > 0$  accounts for the addition of water molecules to the dry polymer in the loaded state. It is convenient to define the volume fraction of the polymer and the liquid phases in the gel via  $c_p = 1/J$  and  $c_l = (J-1)/J$ , respectively.

The free energy-density per unit referential volume associated with the swelling process and the exertion of an external force can be written as

$$\psi = \psi_n + \psi_m + \Pi \left( \frac{1}{c_p} - J \right) + \psi_0. \tag{1}$$

The first contribution in Eq. (1) is the free energy-density per unit referential volume associated with the distortion of the polymer network. In this work, we employ the neo-Hookean model,

$$\psi_n = \frac{G}{2} (I_1 - 3 - 2 \ln J), \qquad (2)$$

where  $I_1 = \operatorname{Tr} \left( \mathbf{F}^T \mathbf{F} \right)$  and G is the shear modulus.

The second contribution in Eq. (1) stems from the mixing process of the liquid and the polymer. Following the works of Flory (1942) and Huggins (1942), we employ the form

$$\psi_m = \frac{k_b T}{V_p} (m \ln c_l + N_0 \ln c_p + \chi m c_p), \qquad (3)$$

where the first two terms account for the entropy of mixing, as modeled by Flory (1942) and Hug-

gins (1942), and the third term stems from enthalpic mechanisms during the swelling process. Broadly, the enthalpy pertains to the heat that is being absorbed or released during the mixing process and motivates the liquid molecules to penetrate or leave the gel. The dimensionless interaction parameter  $\chi$  accounts for the interaction between the polymer and the liquid solvent. Note that Eq. (3) assumes that n > 5 (Cohen and McMeeking, 2019). In addition, since we consider polymer networks that are completely hydrophilic, oil molecules cannot penetrate the gel and are thus not accounted for in Eq. (3). However, the analysis can be expanded to account for hydrophobic interactions as well.

The third term in Eq. (1) enforces the incompressibility of the polymer and the liquid molecules in the gel. The Lagrange multiplier  $\Pi$  is determined from the boundary and the equilibrium conditions and can be understood as the total pressure of the solvent-polymer mixture, which is the sum of the osmotic and the solvent pressure. The last term of Eq. (1) (i.e.  $\psi_0$ ) is the free energy-density per unit referential volume of the dry polymer.

The true (Cauchy) stress tensor can be determined from the free energy-density function (Eq. (1)) via

$$\sigma = \frac{1}{J} \frac{\partial \psi}{\partial \mathbf{F}} \mathbf{F}^T = \frac{G}{J} \left( \mathbf{F} \mathbf{F}^T - \mathbf{I} \right) - \Pi \mathbf{I}, \tag{4}$$

where  ${f I}$  is the identity tensor. The first Piola-Kirchhoff stress is given via  ${f P}=J\,{f \sigma}\,{f F}^{-T}.$ 

The free energy-density function in Eq. (1) also allows to determine the chemical potential of a liquid molecule in the gel network via

$$\mu = \frac{\partial (\psi V_p)}{\partial m} = k_b T \left( \ln c_l + c_p + \chi c_p^2 \right) + \Pi v_l.$$
 (5)

We recall that the chemical potential of a liquid molecule accounts for the change in the free energy resulting from the relocation of one liquid molecule into or out of the gel.

The equilibrium state of the gel requires mechanical equilibrium, i.e.  $\nabla \cdot \boldsymbol{\sigma} = \mathbf{0}$  where the divergence operator is carried out with respect to the current coordinate system. Additionally, the

stress tensor must satisfy the prescribed boundary conditions. To achieve chemical equilibrium, the chemical potential of the liquid molecules inside the gel must be equal to the chemical potential of the solvent, given by  $\mu_l = (\tilde{p} - \tilde{p}_0) v_l$  where  $\tilde{p}_0$  is the liquid pressure in a reference state. Therefore, chemical equilibrium requires that  $\mu = \mu_l$ , where Eq. (5) is used.

In the following, we consider tubular and spherical hydrophilic shells that are filled with either water or oil. In the simulations, we set  $k_b T = 4.1 \cdot 10^{-21} \, \mathrm{J}$  (i.e. room temperature), the shear modulus of the dry polymer  $G = 10^3 \, \mathrm{Pa}$ , and the interaction parameter  $\chi = 0.2$ . We point out that the trends of the responses of the gels are independent of the value of the shear modulus G, and thus we normalize the pressure by the shear modulus. To determine the chemical potential, we recall that the volume of a water molecule is  $v_l = 3 \cdot 10^{-29} \, m^3$  and set  $\tilde{p} = \tilde{p}_0$ .

# 3 Liquid filled tubular gels

We begin by considering a cylindrical polymeric shell that is filled with either oil or water. It is convenient to use a cylindrical coordinate system  $\{\hat{\mathbf{R}}, \hat{\boldsymbol{\Theta}}, \hat{\mathbf{Z}}\}$  to define the material points in the reference configuration such that  $R_i \leq R \leq R_o$ ,  $0 \leq \Theta \leq 2\pi$ , and  $0 \leq Z \leq L$ . Here,  $R_i$  and  $R_o$  denote the inner and the outer radii of the shell, respectively,  $\Theta$  is the polar angle, Z is the longitudinal coordinate, and L is the total length of the cylinder.

The tube swells under a fixed length L such that  $\sigma_{rr}(R=R_i)=0$  and  $\sigma_{rr}(R=R_o)=0$ , where  $\sigma_{rr}$  is the radial stress. We denote the inner and the outer radii in the freely swollen state by  $r_i^{FS}$  and  $r_o^{FS}$ , respectively. Next, we fill the tube with liquid, seal and fix the ends such that no displacements are possible along the  $\hat{\mathbf{Z}}$ -direction, and apply a radial pressure p to the outer surface (see Fig. (2)). Such radial pressure can be generated by an osmotic pressure or cell-generated forces. In the loaded state, the length of the tube remains L and the radius is given by r=r(R).

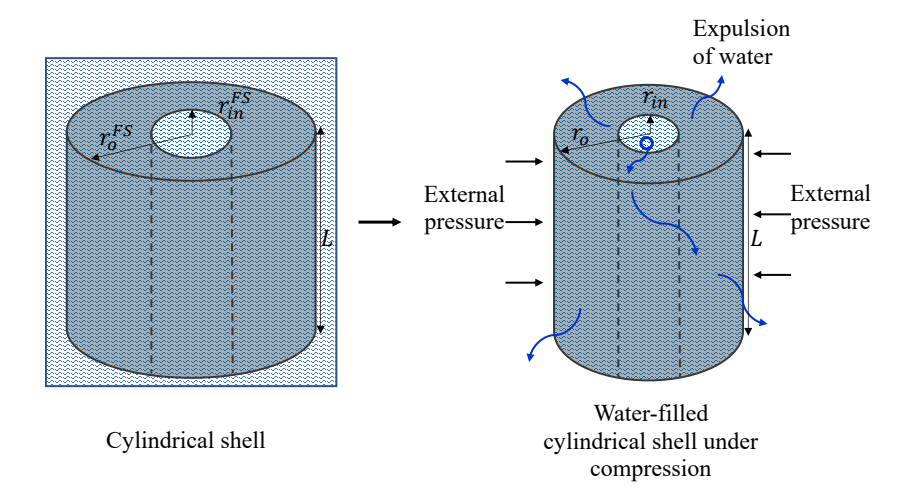


Figure 2: Illustration of a cylindrical shell filled with water under an external pressure. Water molecules can migrate from the core to the hydrogel and escape from the hydrogel to the surrounding environment.

Accordingly, the deformation gradient from the reference to the loaded state can be written as

$$\mathbf{F} = \begin{pmatrix} \frac{\mathrm{d}r}{\mathrm{d}R} & 0 & 0\\ 0 & \frac{r}{R} & 0\\ 0 & 0 & 1 \end{pmatrix}. \tag{6}$$

The mechanical equilibrium equations along the  $\hat{\mathbf{Q}}$  and the  $\hat{\mathbf{Z}}$  directions are satisfied automatically. Equilibrium along the radial direction requires

$$\frac{\partial \sigma_{rr}}{\partial r} + \frac{\sigma_{rr} - \sigma_{\theta\theta}}{r} = 0, \tag{7}$$

where  $\sigma_{\theta\theta}$  is the tangential Cauchy stress component. The mechanical boundary conditions in the loaded state depend on the liquid inside the cylindrical shell, as described in the following. In addition, we require that  $\mu=0$  to satisfy chemical equilibrium.

#### 3.1 Oil filled tubular hydrogel

First, consider a hydrophilic cylindrical hydrogel that is filled with oil. The hydrophobic oil molecules repel the water in the cylindrical hydrogel and therefore maintain a fixed inner radius, i.e.  $r(R=R_i)=r_i^{FS}$ . The externally applied pressure imposes the boundary condition  $\sigma_{rr}(r=R_o)=-p$ . We note that the chemical potential of the oil molecules inside the shell is not necessarily equal to that of the water molecules in the surrounding environment. Rather, forces stemming from hydrophobic-hydrophilic repulsion ensure equilibrium.

Figs. (3a) and (3b) depict the normalized dimensionless pressure p/G and the volumetric deformation  $J_l$  as a function of the outer radial stretch  $r_o/r_o^{FS}$ , respectively, for three geometric ratios  $R_o/R_i=1.1,1.5$ , and 2. We find that the increase in pressure leads to a reduction in the gel volume. Recall that the polymer and the water molecules are assumed to be incompressible and therefore the decrease in volume stems from the expulsion of water molecules from the gel through the outer boundary. To understand this process, note that the chemical potential of the water molecules inside the gel increases with the pressure, thereby motivating an outward diffusion and an overall reduction in volume. As the pressure increases, there are fewer water molecules capable of escaping the gel tube, leading to a more moderate reduction in the radius, and therefore in volume.

The observed trend is similar for the three geometric ratios that are considered here. However, increasing  $R_o/R_i$  allows the diffusion of more water molecules and therefore a larger reduction in the outer radius. Due to the constant inner radius, the volumetric deformations due to the compressive loading are larger for thicker tubes. Additionally, we find that thinner tubes are stiffer in the sense that larger pressures are required to achieve a given radial stretch.

#### 3.2 Water filled hydrogel

Next, we consider a hydrophilic tubular hydrogel filled with a water core. We apply an external pressure on the outer boundary  $\sigma_{rr}$   $(r = R_o) = -p$ . Here, the inner boundary is traction free (i.e.  $\sigma_{rr}$   $(r = R_i) = 0$ ) since any pressure that is transferred to the water inside the tube leads to the

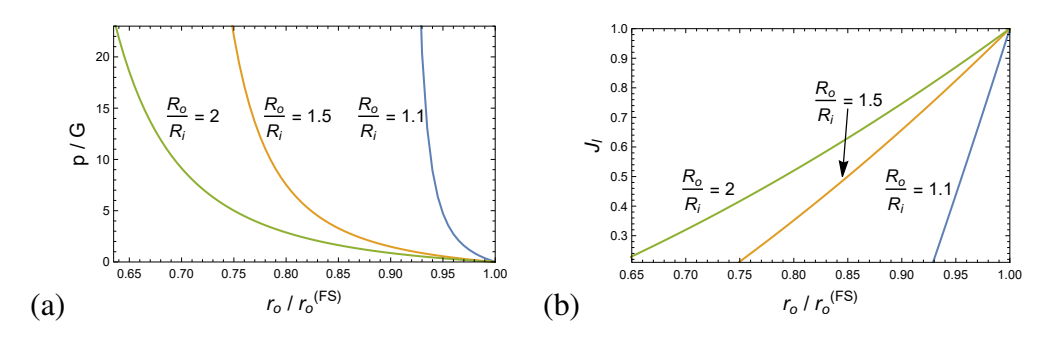


Figure 3: (a) The normalized pressure p/G and (b) the change in the volume  $J_l$  as a function of the outer radial stretch  $r_o/r_o^{FS}$  for an oil filled cylindrical polymeric gel characterized by the outer to inner radius ratio  $R_o/R_i = 1.1, 1.5$ , and 2.

diffusion of water molecules from the inner core to the gel, as depicted in Fig. (2).

Figs. (4a), (4b), and (4c) illustrate the normalized (dimensionless) pressure p/G, the inner radial stretch  $r_i/r_i^{FS}$ , and the volumetric deformation of the swollen network due to the load  $J_l$  as a function of the outer radial stretch  $r_o/r_o^{FS}$ , respectively, for three geometric ratios  $R_o/R_i=1.1$ , 1.5, and 2. Note that we observe a more pronounced decrease in the outer radius stretch  $r_o/r_o^{FS}$  as the external pressure increases in thinner water filled shells; this is exactly opposite of the trend observed in oil filled hydrogel tubes (Fig. (3a)). In addition, thinner tubes experience smaller changes in the stretch of the inner radius  $r_i/r_i^{FS}$  and, consequently, in the volume. This stems from the differences in the initial volumes of the tube, i.e. thinner tubes can uptake less water than thicker tubes.

It is important to emphasize that the kinematic changes observed here stem from a balance between the diffusion of water molecules into and out of the gel through the inner and the outer boundaries, respectively. A comparison between Figs. (4a) and (3a) reveals opposite trends: cylindrical shells can be stiffer or softer if they are filled with oil or water, respectively. In addition, the range of pressures required to deform water-filled hydrogels are much lower due to the possible reduction in the inner radius.

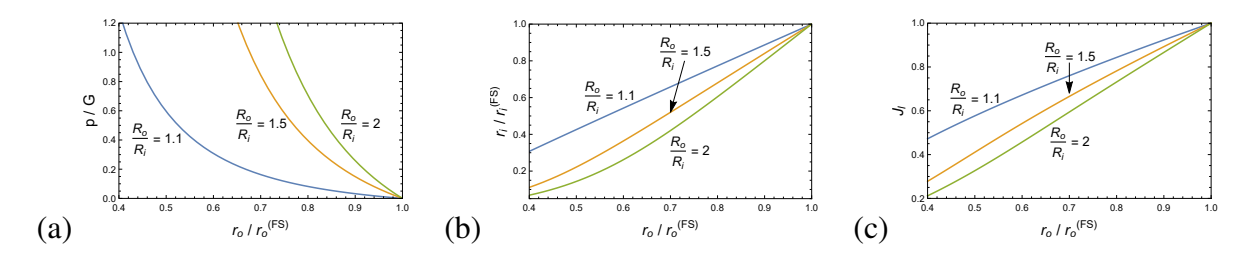


Figure 4: (a) The normalized pressure p/G, (b) the stretch of the inner radius  $r_i/r_i^{FS}$ , and (c) the change in the volume  $J_l$  as a function of the outer radial stretch  $r_o/r_o^{FS}$  for a water filled cylindrical polymeric gel characterized by the outer to inner radius ratio  $R_o/R_i = 1.1, 1.5$ , and 2.

# 4 Liquid filled spherical shell gels

Next, we investigate the response of spherical shells that are filled with either oil or water. To this end, it is convenient to employ a spherical coordinate system  $\left\{\hat{\mathbf{R}},\hat{\boldsymbol{\Theta}},\hat{\boldsymbol{\Phi}}\right\}$  and denote the referential material points  $R_i \leq R \leq R_o$ ,  $0 \leq \Theta \leq \pi$ , and  $0 \leq \Phi < 2\pi$ . Here,  $R_i$  and  $R_o$  denote the radius and the inner and the outer radii of the shell, respectively,  $\Theta$  is the polar angle, and  $\Phi$  is the azimuthal angle.

The spherical shell is allowed to undergo free swelling such that  $\sigma_{rr}$   $(R=R_i)=0$  and  $\sigma_{rr}$   $(R=R_o)=0$ , where  $\sigma_{rr}$  is the radial stress. As before, we denote the inner and the outer radii in the swollen state by  $r_i^{FS}$  and  $r_o^{FS}$ , respectively. Next, we fill the spherical shell with liquid and apply a radial pressure p to the outer surface, as illustrated in Fig. (5). Note that the loading is axisymmetric and we define the radial mapping of the material points via r=r(R). Accordingly, the deformation gradient from the reference to the loaded state can be written as

$$\mathbf{F} = \begin{pmatrix} \frac{\mathrm{d}r}{\mathrm{d}R} & 0 & 0\\ 0 & \frac{r}{R} & 0\\ 0 & 0 & \frac{r}{R} \end{pmatrix}. \tag{8}$$

The mechanical equilibrium equations along the  $\hat{\Theta}$  and the  $\hat{\Phi}$  directions are automatically satisfied with the deformation gradient in Eq. (8). The remaining equilibrium equation along the radial

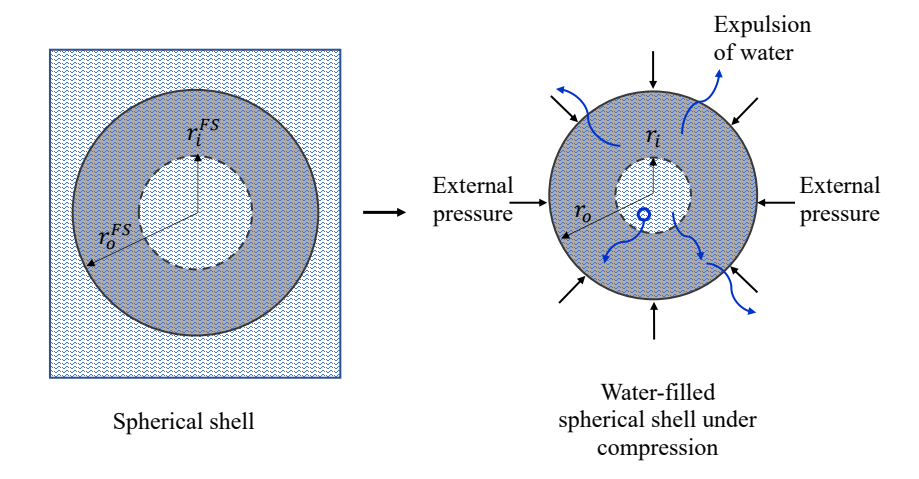


Figure 5: Illustration of a spherical shell filled with water under external pressure.

direction is

$$\frac{\partial \sigma_{rr}}{\partial r} + \frac{2\sigma_{rr} - \sigma_{\theta\theta} - \sigma_{\phi\phi}}{r} = 0, \tag{9}$$

where  $\sigma_{\theta\theta}$  and  $\sigma_{\phi\phi}$  are the polar and the azimuthal Cauchy stress components, respectively.

Once again, we highlight that chemical equilibrium requires that the chemical potential of the water molecules inside the gel are equal to the chemical potential of the water molecules in the surrounding environment, i.e.  $\mu=0$ . This condition must be satisfied in the swollen and the loaded states. The mechanical boundary conditions in the loaded state depend on the liquid inside the spherical shell and are described in the following.

### 4.1 Oil filled spherical shell

We begin by filling the hydrophilic spherical shell gel with oil. Accordingly, the mechanical boundary conditions are given in terms of a fixed inner radius  $r(R=R_i)=r_i^{FS}$  and an externally applied pressure  $\sigma_{rr}(r=R_o)=-p$ .

Figs. (6a) and (6b) plot the normalized (dimensionless) applied pressure p/G and the volumetric deformation  $J_l$  versus the outer radial stretch  $r_o/r_o^{FS}$  for the geometric ratios  $R_o/R_i = 1.1$ ,

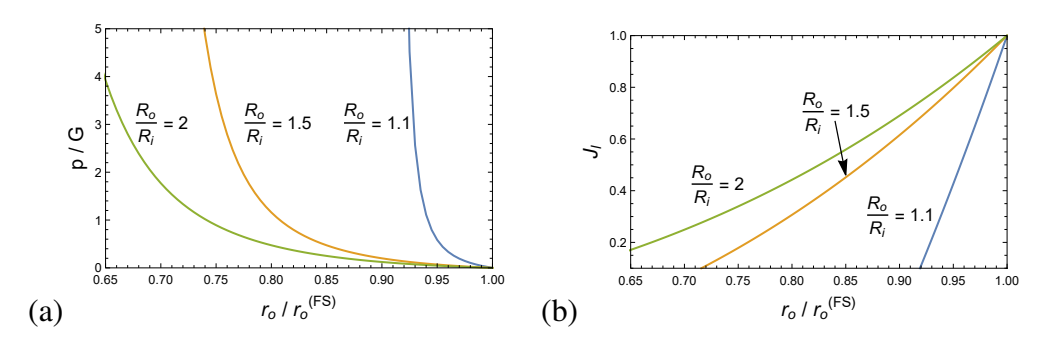


Figure 6: (a) The normalized pressure p/G and (b) the volumetric deformation  $J_l$  as a function of the outer radial stretch  $r_o/r_o^{FS}$  for an oil filled spherical polymeric gel characterized by the outer to inner radius ratio  $R_o/R_i = 1.1, 1.5$ , and 2.

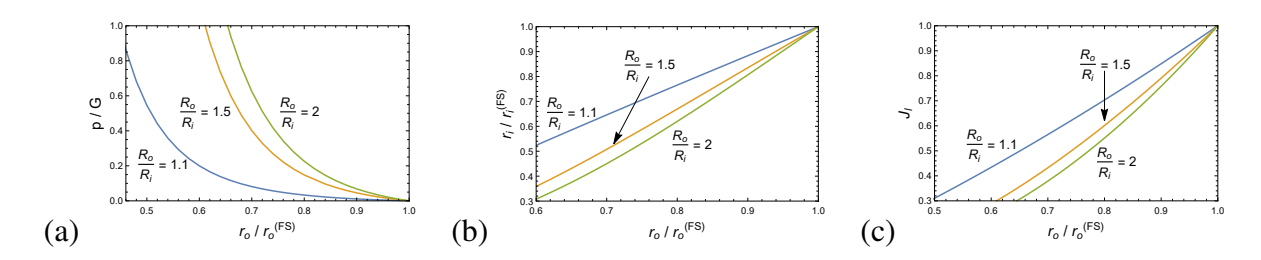


Figure 7: (a) The normalized pressure p/G and (b) the stretch of the inner radius  $r_i/r_i^{FS}$ , and (c) the change in the volume  $J_l$  as a function of the outer radial stretch  $r_o/r_o^{FS}$  for a water filled spherical polymeric gel characterized by the outer to inner radius ratio  $R_o/R_i = 1.1, 1.5$ , and 2.

1.5, and 2. As before, the pressure p motivates the escape of water molecules through the outer boundary. Since the swelling of thinner shells results in a smaller uptake of water molecules, we find that thinner shells are stiffer and experience smaller volumetric deformations under an applied pressure as compared to thicker shells.

Interestingly, comparison of Figs. (6a) and (3a) shows that tubular core-shell gels are stiffer than spherical shells. Consequently, spherical shells experience larger reduction in volume, as can be also concluded by comparing Figs. (6b) and (3b). This effect directly stems from the longitudinal constraints we imposed on the cylindrical gel, which limits its elongation, while the sphere is allowed to contract in all directions.

#### 4.2 Water filled spherical shell

Next, we consider a hydrophilic spherical hydrogel shell filled with water. The mechanical boundary conditions are  $\sigma_{rr}(r=R_o)=-p$ , i.e. the applied pressure on the outer boundary, and  $\sigma_{rr}(r=R_i)=0$ , stemming from the ability of water molecules that are trapped in the core to penetrate into the gel, as showed in Fig. (5).

Figs. (7a), (7b), and (7c) plot the normalized pressure p/G, the inner radial stretch  $r_i/r_i^{FS}$ , and the volumetric deformation  $J_l$  as a function of the outer radial stretch  $r_o/r_o^{FS}$ , respectively, for the three geometric ratios  $R_o/R_i=1.1,\,1.5,\,$  and 2. Similar to the case of the tubular gels, we find opposing trends regarding the geometric effects on the stiffness of water- and oil- filled spherical shells. Specifically, spherical shells with higher  $R_o/R_i$  ratios are softer if they are filled with oil but stiffer if they are filled with water.

Examination of Fig. (7b) shows that the relative decrease in the inner radius is smaller for thin tubes. As a result, thicker tubes experience a larger reduction in volume for the same  $r_o/r_o^{FS}$ , as shown in (7c). To understand this, we recall that the water in the core diffuses into the gel through the inner boundary, thereby increasing the volume of the shell. This increase is counteracted by the expulsion of water molecules through the outer boundary, resulting in a net volume reduction. It is interesting to note that theoretically, a high enough pressure can force all of the water molecules out of the gel, thereby resulting in a much stiffer polymeric sphere.

Comparing Figs. (4c) and (7c) for cylindrical and spherical water filled shells, respectively, reveals a more significant reduction in the volume for spherical shells. This result stems from the longitudinal constraints imposed on the cylindrical shells.

## 5 Conclusions

This work presents a comprehensive study of the mechanical response of hydrogel based core-shell structures. We demonstrate that a compressive loading leads to a reduction in the overall volume

of tubular and spherical hydrogel shells due to the pressure induced expulsion of water molecules from within the hydrogels to the surrounding aqueous environment. The thickness of the shell determines the initial stiffness and the overall behavior of the core-shell system. Spherical and the tubular hydrogel shells exhibit similar trends under compressive loading. However, tubular gels are stiffer due to the imposed longitudinal constraints that are enforced, whereas spherical shells contract in all directions and experience larger volumetric deformations. This result suggests that the choice of shell geometry can be used to enhance the performance of hydrogels as vehicles for the delivery of drugs or other payloads.

The liquid core composition is also critical to the stiffness and the overall behavior of the hydrogel system. In oil filled systems, thinner shells experience a moderate reduction in the gel volume, as the inner radius is fixed due to the repulsion between oil and water molecules. By contrast, the inner radius of water-filled cylindrical shells significantly contracts under a compressive load. This phenomenon stems from the transportation of water molecules from the inner aqueous core to the hydrophilic shell. We point out that during this process, some water molecules escape the shell towards the surrounding environment to comply with the chemical equilibrium conditions. Interestingly, in water filled core-shell structures thinner shells experience higher stretches than thicker tubes and are softer. While this work focused on purely hydrophilic polymers, it can be easily amended to account for hydrophobic or a mixture of hydrophobic/hydrophilic gels. Our results serve as a design guide that can be used to enhance the performance of gels in various applications, including cell-based sensors with tunable mechanical response, drug-loaded vehicles capable of compression-induced delivery, and bio-compatible materials for use in wound healing, tissue replacement, and cell encapsulation for regenerative therapies.

**Acknowledgments** This research was primarily supported by a grant from the United States-Israel Binational Science Foundation (BSF, grant number 2019742), Jerusalem, Israel, and the United States National Science Foundation (NSF, grant number DMR-2004937). This work was partially supported by the MRSEC Program of the National Science Foundation under Award No.

DMR 1720256 (IRG-3).

## **References**

- Ullah, F., Othman, M. B. H., Javed, F., Ahmad, Z., and Akil, H. M. (2015) Classification, processing and application of hydrogels: A review. *Materials Science and Engineering: C* 57, 414–433.
- Varaprasad, K., Raghavendra, G. M., Jayaramudu, T., Yallapu, M. M., and Sadiku, R. (2017) A mini review on hydrogels classification and recent developments in miscellaneous applications.
  Materials Science and Engineering: C 79, 958–971.
- Flory, P. J. Principles of polymer chemistry; Cornell Univ Press: Ithaca, NY, 1953.
- Cohen, N., and McMeeking, R. M. (2019) On the swelling induced microstructural evolution of polymer networks in gels. *Journal of the Mechanics and Physics of Solids* 125, 666 680.
- Boateng, J. S., Matthews, K. H., Stevens, H. N., and Eccleston, G. M. (2008) Wound healing dressings and drug delivery systems: a review. *Journal of pharmaceutical sciences* 97, 2892–2923.
- Kamoun, E. A., Kenawy, E.-R. S., and Chen, X. (2017) A review on polymeric hydrogel membranes for wound dressing applications: PVA-based hydrogel dressings. *Journal of advanced research* 8, 217–233.
- Gupta, A., Kowalczuk, M., Heaselgrave, W., Britland, S. T., Martin, C., and Radecka, I. (2019) The production and application of hydrogels for wound management: A review. *European Polymer Journal* 111, 134–151.
- Lee, K. Y., and Mooney, D. J. (2001) Hydrogels for tissue engineering. *Chemical reviews 101*, 1869–1880.

- Drury, J. L., and Mooney, D. J. (2003) Hydrogels for tissue engineering: scaffold design variables and applications. *Biomaterials* 24, 4337–4351.
- Hoffman, A. S. (2012) Hydrogels for biomedical applications. *Advanced drug delivery reviews* 64, 18–23.
- Jagur-Grodzinski, J. (2006) Polymers for tissue engineering, medical devices, and regenerative medicine. Concise general review of recent studies. *Polymers for Advanced Technologies* 17, 395–418.
- Li, J., and Mooney, D. J. (2016) Designing hydrogels for controlled drug delivery. *Nature Reviews Materials* 1, 1–17.
- Graham, N., and McNeill, M. (1984) Hydrogels for controlled drug delivery. *Biomaterials* 5, 27–36.
- Gupta, P., Vermani, K., and Garg, S. (2002) Hydrogels: from controlled release to pH-responsive drug delivery. *Drug discovery today* 7, 569–579.
- Duncan, R. (2003) The dawning era of polymer therapeutics. *Nature Reviews Drug Discovery* 2, 347.
- Dreiss, C. A. (2020) Hydrogel design strategies for drug delivery. *Current Opinion in Colloid & Interface Science* 48, 1–17.
- Xu, L., Guo, Y., Huang, Y., Xu, Y., Lu, Y., and Wang, Z. (2019) Hydrogel materials for the application of islet transplantation. *Journal of biomaterials applications* 33, 1252–1264.
- Wang, L., Neumann, M., Fu, T., Li, W., Cheng, X., and Su, B.-L. (2018) Porous and responsive hydrogels for cell therapy. *Current Opinion in Colloid & Interface Science* 38, 135–157.
- Choe, G., Park, J., Park, H., and Lee, J. Y. (2018) Hydrogel biomaterials for stem cell microencapsulation. *Polymers* 10, 997.

- Burdick, J. A., Mauck, R. L., and Gerecht, S. (2016) To serve and protect: hydrogels to improve stem cell-based therapies. *Cell stem cell 18*, 13–15.
- Banerjee, A., Arha, M., Choudhary, S., Ashton, R. S., Bhatia, S. R., Schaffer, D. V., and Kane, R. S. (2009) The influence of hydrogel modulus on the proliferation and differentiation of encapsulated neural stem cells. *Biomaterials* 30, 4695–4699.
- Lee, J., Abdeen, A. A., Zhang, D., and Kilian, K. A. (2013) Directing stem cell fate on hydrogel substrates by controlling cell geometry, matrix mechanics and adhesion ligand composition. *Biomaterials* 34, 8140–8148.
- Engler, A. J., Sen, S., Sweeney, H. L., and Discher, D. E. (2006) Matrix elasticity directs stem cell lineage specification. *Cell* 126, 677–689.
- Ribeiro, A. J., Denisin, A. K., Wilson, R. E., and Pruitt, B. L. (2016) For whom the cells pull: Hydrogel and micropost devices for measuring traction forces. *Methods 94*, 51–64.
- Huang, J., Wang, L., Xiong, C., and Yuan, F. (2016) Elastic hydrogel as a sensor for detection of mechanical stress generated by single cells grown in three-dimensional environment. *Biomaterials* 98, 103–112.
- Roca-Cusachs, P., Conte, V., and Trepat, X. (2017) Quantifying forces in cell biology. *Nature cell biology* 19, 742–751.
- Vorselen, D., Wang, Y., de Jesus, M. M., Shah, P. K., Footer, M. J., Huse, M., Cai, W., and Theriot, J. A. (2020) Microparticle traction force microscopy reveals subcellular force exertion patterns in immune cell-target interactions. *Nature Communications* 11, 20.
- Mendez, M. G., and Janmey, P. A. (2012) Transcription factor regulation by mechanical stress. *The international journal of biochemistry & cell biology 44*, 728–732.

- Uroz, M., Wistorf, S., Serra-Picamal, X., Conte, V., Sales-Pardo, M., Roca-Cusachs, P., Guimerà, R., and Trepat, X. (2018) Regulation of cell cycle progression by cell–cell and cell–matrix forces. *Nature cell biology* 20, 646–654.
- Franck, C., Maskarinec, S. A., Tirrell, D. A., and Ravichandran, G. (2011) Three-dimensional traction force microscopy: a new tool for quantifying cell-matrix interactions. *PloS one* 6, e17833.
- Huang, J., Deng, H., Peng, X., Li, S., Xiong, C., and Fang, J. (2012) Cellular traction force reconstruction based on a self-adaptive filtering scheme. *Cellular and Molecular Bioengineering 5*, 205–216.
- Munevar, S., Wang, Y.-l., and Dembo, M. (2001) Traction force microscopy of migrating normal and H-ras transformed 3T3 fibroblasts. *Biophysical journal* 80, 1744–1757.
- Mohagheghian, E., Luo, J., Chen, J., Chaudhary, G., Chen, J., Sun, J., Ewoldt, R. H., and Wang, N. (2018) Quantifying compressive forces between living cell layers and within tissues using elastic round microgels. *Nature Communications* 9, 1878.
- Kaytanlı, B., Khankhel, A. H., Cohen, N., and Valentine, M. T. (2020) Rapid analysis of cell-generated forces within a multicellular aggregate using microsphere-based traction force microscopy. *Soft matter 16*, 4192–4199.
- Xu, S., and Nisisako, T. (2020) polymer capsules with tunable Shell thickness Synthesized via Janus-to-core shell transition of Biphasic Droplets produced in a Microfluidic Flow-Focusing Device. *Scientific reports* 10, 1–10.
- Nisisako, T., and Hatsuzawa, T. (2016) Microfluidic fabrication of oil-filled polymeric microcapsules with independently controllable size and shell thickness via Janus to core–shell evolution of biphasic droplets. *Sensors and Actuators B: Chemical* 223, 209–216.

- Ran, R., Sun, Q., Baby, T., Wibowo, D., Middelberg, A. P., and Zhao, C.-X. (2017) Multiphase microfluidic synthesis of micro-and nanostructures for pharmaceutical applications. *Chemical Engineering Science* 169, 78–96.
- Mahdavi, Z., Rezvani, H., and Moraveji, M. K. (2020) Core-shell nanoparticles used in drug delivery-microfluidics: a review. *RSC Advances 10*, 18280–18295.
- Drozdov, A. D. (2015) Equilibrium swelling of core-shell composite microgels. *Meccanica* 50, 1579–1592.
- Cohen, N. (2019) Programming the equilibrium swelling response of heterogeneous polymeric gels. *International Journal of Solids and Structures* 178-179, 81 90.
- Levin, M., and Cohen, N. (2021) The effects of aging on the mechanical properties of the vitreous. *Journal of Biomechanics* 110310.
- Flory, P. J. (1942) Thermodynamics of High Polymer Solutions. *The Journal of Chemical Physics* 10, 51–61.
- Huggins, M. L. (1942) Thermodynamic properties of solutions of long-chain compounds. *Annals of the New York Academy of Sciences 43*, 1–32.